Chemical Science

ROYAL SOCIETY OF CHEMISTRY

EDGE ARTICLE

View Article Online
View Journal | View Issue

Cite this: *Chem. Sci.*, 2021, **12**, 12346

All publication charges for this article have been paid for by the Royal Society of Chemistry

Surface chiroselective assembly of enantiopure crystalline porous films containing bichiral building blocks†

Hao Chen,[ac] Zhi-Gang Gu *[abc] and Jian Zhang *[abc]

Received 8th June 2021
Accepted 14th August 2021

DOI: 10.1039/d1sc03089b

rsc.li/chemical-science

The development of chiral crystalline porous materials (CPMs) containing multiple chiral building blocks plays an important role in chiral chemistry and applications but is a challenging task. Herein, we report the first example of bichiral building block based enantiopure CPM films containing metal–organic cages (MOCs) and metal complexes. The functionalized substrate was immersed subsequently into homochiral metal complex (*R*)- or (*S*)-Mn(DCH)$_3$ (DCH = 1,2-diaminocyclohexane) and racemic Ti_4L_6 cage (L = embonate) solutions by a layer-by-layer growth method. During the assembly process, the substrate surface coordinated with (*R*)- or (*S*)-Mn(DCH)$_3$ can, respectively, layer-by-layer chiroselectively connect Δ- or Λ-Ti_4L_6 cages to form homochiral (*R*, Δ)- or (*S*, Λ)-CPM films with a preferred [111] growth orientation, tunable thickness and homogeneous surface. The resulting enantiopure CPM films show strong chirality, photoluminescence, and circularly polarized luminescence (CPL) properties as well as good enantioselective adsorption toward enantiomers of 2-butanol and methyl-lactate. The present *in situ* surface chiroselective strategy opens a new route to assemble homochiral CPM films containing multiple chiral building blocks for chiral applications.

Introduction

The development of chiral materials has attracted great attention to their potential applications in the pharmaceutical,[1] agricultural,[2] chemical and biological fields.[3–6] As emerging chiral materials, chiral crystalline porous materials (CPMs) including metal–organic frameworks (MOFs),[7–10] covalent–organic frameworks (COFs)[11–13] and supramolecular–organic frameworks (SOFs)[14–16] possess high specific surface area, well-defined pores and variable chemical functionalities. Chiral CPMs have been rapidly expanded in enantiomer separation,[17–22] asymmetric catalysis,[23–26] nonlinear optics,[27] circularly polarized luminescence (CPL),[28,29] drug delivery[30,31] and chiral sensing.[32–34] Compared with powder materials, the form of film or membrane is more favorable in the applications.[35–38] Despite some chiral CPM films having been reported, usually they only contain one chiral building block.[39–42] Multiple chiral building blocks can easily promote the formation of hierarchical and multichiral pore structures with multiple functions in the field of asymmetric synthesis and enantiomeric recognition.[43–46] Therefore, the development of a new class of enantiopure CPM films containing multiple chiral building blocks is important but still a big challenge.

Metal–organic cages (MOCs) with specific configurations and functions have emerged as an appealing topic in recent coordination chemistry.[47–49] MOCs with unique geometries and large inner voids can be employed as building blocks to construct CPMs with a hierarchical pore structure through a variety of coordination and supramolecular interactions, which provide potential applications in the fields of adsorption/separation, heterogeneous catalysis, drug release, and mimicry of biological processes.[3,16,35–37] In particular, tetrahedral MOCs (M_4L_6 or M_4L_4-type) as typical polyhedral structures, are ideal secondary building units (SBUs) to further construct CPMs.[2,50–52] However, synthesis of enantiopure CPMs based on tetrahedral MOCs is difficult due to tetrahedral MOCs usually existing in both forms of enantiomers (ΔΔΔΔ and ΛΛΛΛ).[23,53] Particularly, the assembly of their enantiopure CPM films is challenging and has not been reported to date.

Herein, we report a new homochiral crystalline porous film containing bichiral building blocks by using a layer-by-layer (lbl) assembly strategy. As shown in Scheme 1 and Fig. S4,† the functionalized substrate was immersed subsequently into (*R*)-Mn(DCH)$_3$ or (*S*)-Mn(DCH)$_3$ (DCH = 1,2-diaminocyclohexane) and racemic MOCs[23] (Ti_4L_6 cages, L = embonate) (Fig. S1†) by using an LPE layer-by-layer approach. During the layer-by-layer assembly process, the enantiomer Δ- or Λ-Ti_4L_6 cages

[a]*State Key Laboratory of Structural Chemistry, Fujian Institute of Research on the Structure of Matter, Chinese Academy of Sciences, Fuzhou, Fujian 350002, P. R. China. E-mail: zggu@fjirsm.ac.cn; zhj@fjirsm.ac.cn*

[b]*Fujian Science & Technology Innovation Laboratory for Optoelectronic Information of China, Fuzhou, Fujian 350108, P. R. China*

[c]*University of Chinese Academy of Sciences, Beijing 100049, P. R. China*

† Electronic supplementary information (ESI) available. See DOI: 10.1039/d1sc03089b

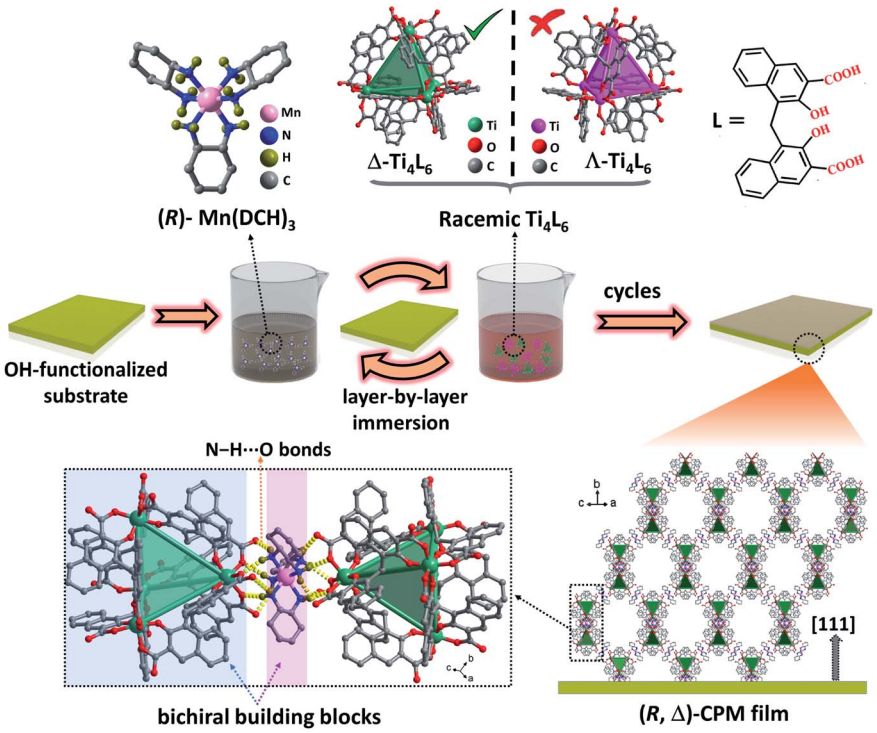

Scheme 1 The preparation of (*R*, Δ)-CPM films by the layer-by-layer chiroselective assembly strategy.

can be chiroselectively coordinated by enantiopure (*R*)-$Mn(DCH)_3$ or (*S*)-$Mn(DCH)_3$, respectively, in each step. Finally, enantiopure (*R*, Δ)- and (*S*, Λ)-CPM films containing metal complexes and MOCs were grown on the substrate surfaces, and they possessed controllable orientation, tunable thickness and a homogeneous surface. Significantly, (*R*, Δ)- and (*S*, Λ)-CPM films display a three-dimensional supramolecular architecture with large diamondoid cages constructed from Ti_4L_6 cages and (*R*)- or (*S*)-Mn-$(DCH)_3$ units *via* N–H···O hydrogen bonds (Fig. S2 and S3†).[53] Circular dichroism (CD), photoluminescence and circularly polarized luminescence (CPL) spectra revealed that the obtained (*R*, Δ)- and (*S*, Λ)-CPM films had strong chirality, photoluminescent emission and CPL. Meanwhile, a vapor adsorption experiment carried out using the quartz crystal microbalance (QCM) technique indicated that the obtained CPM films had high enantioselective adsorption toward enantiomers of 2-butanol and methyl lactate.

Results and discussion

The homochiral (*R*, Δ)-CPM film was grown on hydroxyl-functionalized quartz glass by an LPE automatic dipping method (Scheme 1).[27,54–56] In brief, the –OH functionalized quartz substrate was immersed in (*R*)-$Mn(DCH)_3$ and racemic Ti_4L_6 cage ethanolic solutions sequentially by an automatic dipping LPE lbl method, and the substrate was washed with ethanol to remove residual reactants in each step. During the epitaxial layer-by-layer growth process, the first layer was assembled from the connection of (*R*)-$Mn(DCH)_3$ with the hydroxyl group functionalized surface by N–H···O hydrogen bonds. Then the (*R*)-$Mn(DCH)_3$ selectively coordinated Δ-Ti_4L_6 cages *via* N–H···O hydrogen bonds and formed (*R*, Δ)-CPM film on the substrate surface. The Λ-Ti_4L_6 and redundant Δ-Ti_4L_6 were washed away with ethanol. QCM frequency was *in situ* recorded during the layer-by-layer growth process of the (*R*, Δ)-CPM film. In Fig. 1b, the QCM profiles demonstrated the stepwise and continuous growth of the (*R*, Δ)-CPM film on the QCM substrate with a flowing layer by layer method, which showed that the chiral films can be continuously grown on the surface step by step. Similarly, (*R*)-$Mn(DCH)_3$ was replaced with (*S*)-$Mn(DCH)_3$ and used to assemble (*S*, Λ)-CPM film with the same procedure (Fig. S4†). 30 LPE cycles of the (*R*, Δ)- and (*S*, Λ)-CPM films were used for further characterization and study.

The XRD pattern (Fig. 1a) showed three obvious diffraction peaks at 3.2°, 6.4° and 9.6° corresponding to (111), (222) and (333) peaks in the obtained (*R*, Δ)- and (*S*, Λ)-CPM films, which clearly demonstrated that [111]-oriented crystalline films were formed. In Fig. S5,† the IR absorption bands of the (*R*, Δ)-CPM film at 3068, 1642 and 1359 cm^{-1} can be observed, corresponding to =C–H, C=O, and C–O stretching bands of Ti_4L_6 cages. In addition, the IR absorbance bands at 1250, 2850–2930, and 3233 cm^{-1} were ascribed to C–N, $–CH_2$ and $–NH_2$ vibrations of (*R*)-$Mn(DCH)_3$, respectively. Interestingly, the IR vibration of the $–NH_2$ group at 3233 cm^{-1} in the (*R*, Δ)-CPM film showed a red-shift compared with those of (*R*)-DCH (3357 and 3283 cm^{-1}), which can be attributed to the formation of N–H···O hydrogen bonds between the two precursors.[57] The results indicated that the preparation of the (*R*, Δ)-CPM film was successful. Moreover, the UV-vis absorption spectra (Fig. S6†) of (*R*, Δ)-CPM film showed two characteristic peaks at ~300 and

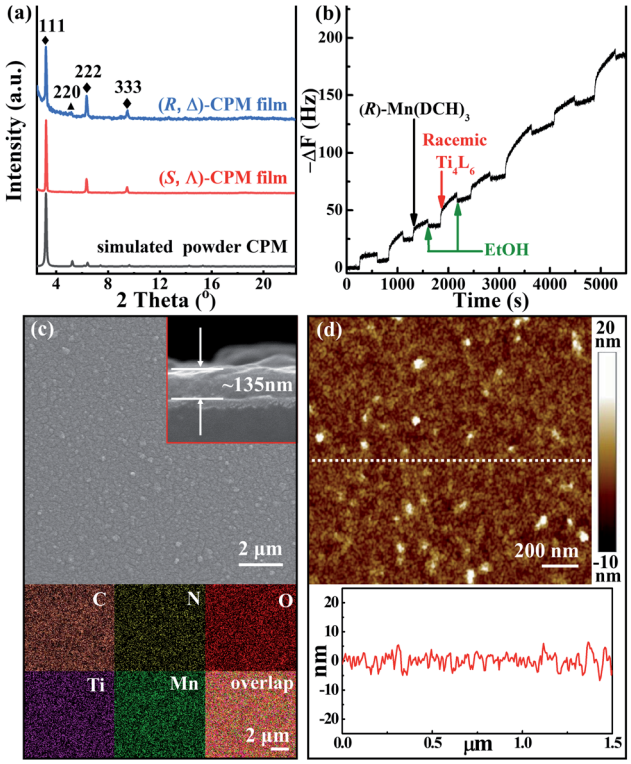

Fig. 1 (a) The XRD patterns of (*R*, Δ)- and (*S*, Λ)-CPM films and calculated XRD of powder CPM; (b) QCM frequency *in situ* recorded during the layer-by-layer growth of (*R*, Δ)-CPM on the QCM substrate; SEM and cross-sectional (inset) images with elemental mapping (c) and AFM image with roughness (d) of the (*R*, Δ)-CPM film.

~360 nm. The surface morphology of the (*R*, Δ)-CPM film was observed from scanning electron microscopy (SEM) images, SEM elemental mapping (Fig. 1c) and an atomic force microscopy (AFM) image (Fig. 1d), showing a homogeneous surface and compact film. In addition, the cross-sectional SEM image (Fig. 1c inset) showed that the thickness of the (*R*, Δ)-CPM film with 30 LPE cycles was ~135 nm. The SEM EDS (Fig. S7†) and ICP of the (*R*, Δ)-CPM film indicated the existence of Ti and Mn. Moreover, the atom ratio of Ti/Mn was ~2, which was consistent with the simulated value in (*R*, Δ)-CPM.

X-ray photoelectron spectroscopy (XPS) was carried out to further investigate the chemical composition and chemical valences of the samples, revealing the presence of C, N, O, Ti and Mn elements in the (*R*, Δ)-CPM film (Fig. S8†). The Ti 2p XPS peaks (Fig. S9†) were ascribed to Ti $2p_{3/2}$ (458.5 eV) and Ti $2p_{1/2}$ (464.6 eV), respectively, owing to the Ti^{4+} in the sample. The two main peaks in the Mn 2p XPS spectrum (Fig. S9†) corresponded to Mn $2p_{3/2}$ and Mn $2p_{1/2}$ in the range of 635–660 eV. In addition, the Mn $2p_{3/2}$ spectrum can be deconvoluted into three distinguished peaks at 640.1, 642.2 and 644.7 eV, which can be ascribed to Mn^{2+}, Mn^{3+} and Mn^{4+}, respectively. The existence of a little Mn^{3+} and Mn^{4+} was ascribed to surface oxidation of the CPM films.[58]

To study the chirality of CPM films grown on quartz glasses, (*R*, Δ)- and (*S*, Λ)-CPM-*x* (*x* = 20, 30 and 40 LPE cycles) films were prepared, respectively. The results revealed that (*R*, Δ)-CPM films with different LPE cycles had smooth, continuous and uniform surfaces (Fig. S10†). The thicknesses of (*R*, Δ)-CPM films were ~92, ~135 and ~166 nm for 20, 30 and 40 cycles, showing an approximately linear relationship with LPE cycles (Fig. S11†). In Fig. 2, the CD spectra showed two negative bands at 264 and 360 nm and a positive band at 294 nm for all (*R*, Δ)-CPM-*x* (*x* = 20, 30 and 40) films. It should be noted that the CD and UV-vis spectrum intensity of (*R*, Δ)- or (*S*, Λ)-CPM films increased with increasing LPE cycles. In particular, the CD peak at 360 nm of (*R*, Δ)-CPM films prepared with different cycles exhibited a nonlinear increase with increasing LPE cycles (Fig. S12†). The results showed that (*R*, Δ)-CPM films can be successfully prepared, and the thickness of films can be well controlled. Moreover, the enantiomeric (*S*, Λ)-CPM films showed that the intensity of CD peaks was nearly equal in magnitude but had opposite signals. In addition, the peak positions of CD signals of CPM films were consistent with those of powder CPM (Fig. S13†).

To further explore the origin of the chiral signal in CPM films, the CD signals of (*R*)- and (*S*)-DCH, and (*R*)- and (*S*)-$Mn(DCH)_3$ were collected. (*R*)- and (*S*)-DCH showed a pair of strong but opposite CD signals at about 242 nm, while (*R*)- and (*S*)-$Mn(DCH)_3$ have no CD signal (Fig. S14†). It is speculated that Mn ions coordinated (*R*)- or (*S*)-DCH successfully to form asymmetric propeller structures on the substrate surface, and further provided a chiral selective seeding layer during the LPE lbl growth process. Therefore, (*R*)- and (*S*)-$Mn(DCH)_3$ can chiroselectively connect with racemic Ti_4L_6 cages to form (*R*, Δ)- and (*S*, Λ)-CPM films. The results showed that the chiral signal of (*R*, Δ)- and (*S*, Λ)-CPM films came from the Δ- or Λ-Ti_4L_6 cages.

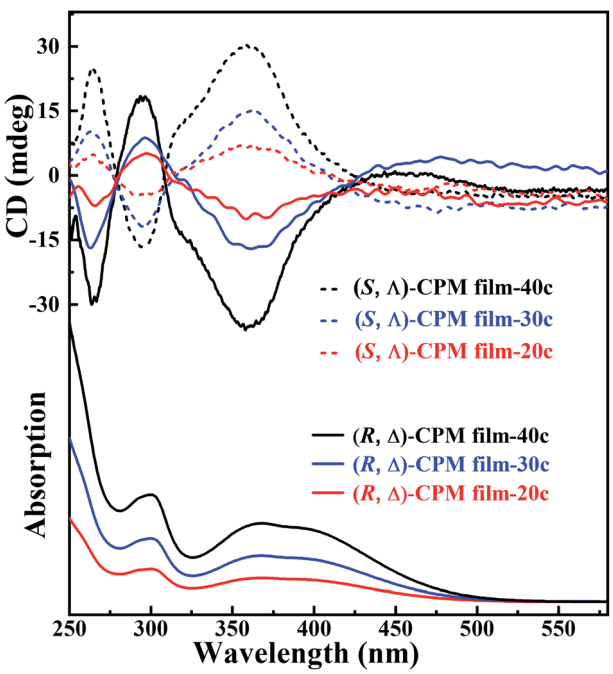

Fig. 2 The CD spectra of (*R*, Δ)- and (*S*, Λ)-CPM-*x* (*x* = 20, 30 and 40 LPE cycles) films for different LPE cycles (above); the UV-vis spectra of (*R*, Δ)-CPM-*x* films (below).

CPL pertains to the excited-state chirality of chiral emitters, which depends on the chirality and fluorescence of materials. CPL spectra of (*R*, Δ)- and (*S*, Λ)-CPM films grown on quartz glasses were further studied at room temperature. In Fig. 3b, the CPL signals with different handedness and emission can be seen clearly. The (*R*, Δ)-CPM film exhibited a negative Cotton effect with a negative CPL peak, while the (*S*, Λ)-CPM film displayed a positive CPL peak. Moreover, the photoluminescence spectra (PL) (Fig. 3a) of (*R*, Δ)- and (*S*, Λ)-CPM films showed peaks at ~530 nm which were consistent with the CPL emission peaks. Their corresponding g_{lum} factors (Fig. S15†) were $\sim -1.8 \times 10^{-3}$ and 2.2×10^{-3} for (*R*, Δ)- and (*S*, Λ)-CPM films, respectively.

To study the enantiomeric recognition of (*R*, Δ)- and (*S*, Λ)-CPM films, the adsorption performance of enantiomers was studied in this work. A gas phase QCM technology was developed for investigating the enantioselectivity of homochiral CPM film, which can monitor mass changes in the nanogram range by detecting the change of resonance frequency. The (*R*, Δ)- or (*S*, Λ)-CPM films were grown on Au-coated QCM sensors by the LPE lbl method. A pair of enantiomers *R*- and *S*-2-butanol were selected as the chiral probe molecules for studying the enantioselectivity of (*R*, Δ)- or (*S*, Λ)-CPM films. The related adsorption amount of *R* and *S*-2-butanol for (*R*, Δ)- or (*S*, Λ)-CPM films was studied, respectively, and the results are shown in Fig. 4a and b. The adsorption amounts of *R*- and *S*-2-butanol for the (*R*, Δ)-CPM film were ~1.11 (*mR*) and ~1.81 (mS) μg cm^{-2}, respectively (Fig. 4a and c). The different adsorption capacities showed an enantioselective adsorption for one 2-butanol enantiomer in (*R*, Δ)-CPM film. When we applied eqn (1) to analyze the enantioselectivity, the enantioselectivity e of the (*R*, Δ)-CPM film for *R*- and *S*-2-butanol was found to be 24.0% (Fig. 4d). With the same measurement, the probe enantiomers of *R*- and *S*-2-butanol were used for studying the enantioselective adsorption of (*S*, Λ)-CPM film. The recorded data (Fig. 4b and c) showed that the adsorption amounts of *R*- and *S*-2-butanol were ~1.24 (m_R) and ~0.77 (m_S) μg cm^{-2} for the (*S*, Λ)-CPM film, respectively. The enantioselectivity e of the (*S*, Λ)-CPM film for *R*- and *S*-2-butanol was 23.4%, which showed contrasting enantioselective adsorption behavior of the (*R*, Δ)-CPM film. These results demonstrated the remarkable enantioselectivity of the (*R*, Δ)-CPM film toward *S*-2-butanol over *R*-2-butanol. In contrast, the (*S*, Δ)-CPM film can selectively recognize *R*-2-butanol.

$$e = (m_R - m_S)/(m_R + m_S) \times 100\% \quad (1)$$

where *e* denotes the enantioselectivity and m_R and m_S are the uptakes of *R*-form and *S*-form enantiomers, respectively.

Homochiral aliphatic compounds are important intermediates in the synthesis of chiral drugs. To further study the enantiomeric aliphatic compound recognition of (*R*, Δ)- and (*S*, Λ)-CPM films, the adsorption performance of D- and L-methyl lactate was explored. The adsorption amounts of D- and L-methyl lactate for the (*R*, Δ)-CPM film were ~0.657 (m_D) and ~1.085 (m_L) μg cm^{-2}, respectively (Fig. S16a and c†). When we applied eqn (1) to analyze the enantioselectivity, the enantioselectivity *e* of the (*R*, Δ)-CPM film for D- and L-methyl lactate was found to be 24.6% (Fig. S16d†). Similarly, the adsorption amounts of D- and L-methyl lactate for the (*S*, Λ)-CPM film were ~1.136 (m_D) and

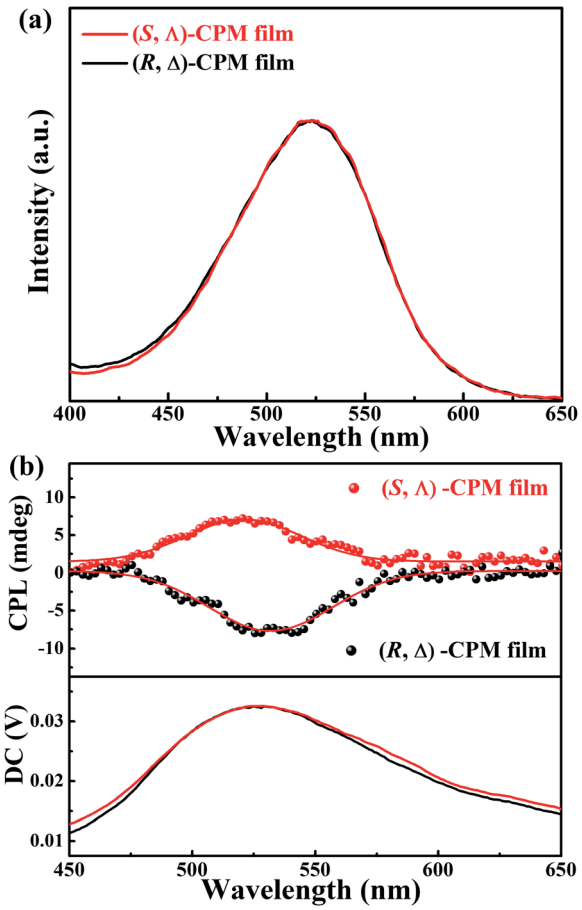

Fig. 3 PL (a) and CPL (b) spectra of (*R*, Δ)- and (*S*, Λ)-CPM films (excitation at 365 nm).

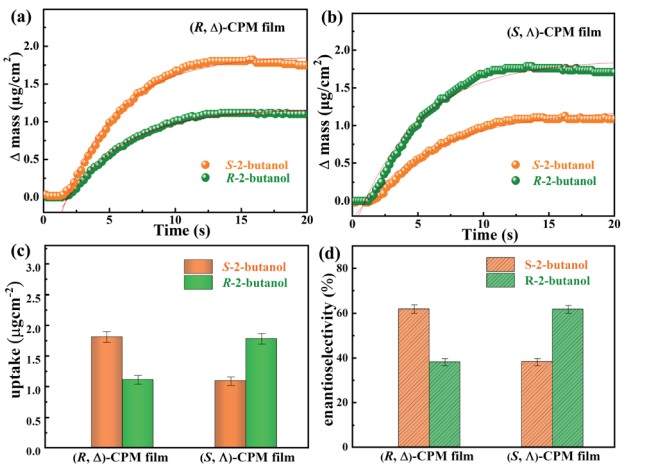

Fig. 4 Mass uptakes of *R*- and *S*-2-butanol in (*R*, Δ)- (a) and (*S*, Λ)-CPM films (b) determined using a gas phase QCM technique; mass uptakes (c) and enantioselectivity (d) of *R*- and *S*-2-butanol in (*R*, Δ)- and (*S*, Λ)-CPM films.

~0.672 (m_L) μg cm^{-2}, respectively (Fig. S16b and c†). The enantioselectivity e of the (*S*, Λ)-CPM film for D- and L-methyl lactate was found to be 25.7% (Fig. S16d†). These results showed that (*R*, Δ)- and (*S*, Λ)-CPM films had sensitive recognition toward enantiomers of L- and D-methyl lactate.

Conclusions

In summary, we have successfully synthesized bichiral building block based homochiral CPM films containing metal–organic cages and metal complexes. By using a liquid-phase epitaxial layer-by-layer assembly process, the racemic Ti_4L_6 cages were selectively coordinated by the substrate surface with *R*- or *S*-Mn(DCH)$_3$ to form (*R*, Δ)- or (*S*, Λ)-CPM films. The obtained CPM films exhibited oriented crystallinity, a homogeneous surface and controllable thickness. The enantiopure CPM films showed obvious CD and CPL signals and green photoluminescent properties as well as good enantioselective adsorption toward enantiomers methyl lactate and 2-butanol. This work provides a new strategy for preparation of enantiopure CPM films containing multiple chiral building blocks from surface chiroselective assembly, which is beneficial for research on chiral chemistry, and the applications in chiral recognition and separation as well as chiral optical devices.

Experimental

Materials and instrumentation

All reagents and solvents employed were commercially available and used as received without further purification. The samples grown on a functionalized Au substrate were characterized with IRRAS. IRRAS data were recorded using a Bruker Vertex 70 FTIR spectrometer. Powder XRD (PXRD) analysis was performed on a MiniFlex2 X-ray diffractometer using Cu Kα radiation (λ = 0.1542 nm) in the 2θ range of 3–25° with a scanning rate of 0.5° min^{-1}. CD experiments were conducted with a Biologic MOS-450 CD spectrometer at room temperature. CD spectra were recorded from 600 to 250 nm in 1 nm steps using a scan speed of 20 nm min^{-1}. CPL spectra were obtained using JASCO CPL-300 spectrophotometers. The quartz substrate was used as the reference of the CD and CPL measurements. The samples were fixed on the instrument directly and perpendicular to the light beam during the measurement. The background spectra from the quartz substrates were subtracted to obtain the final processed CD and CPL spectra. SEM images for the morphology of films were measured using a Zeiss Gemini SEM 300. The UV-vis spectra for the samples were measured using a Lambda 365. The photoluminescence spectra were measured using an Edinburgh Instruments FLS920.

Synthesis of racemic Ti_4L_6 cages[23]

Ti(OiPr)$_4$ (160 μL, 0.50 mmol), H_4L (L = embonate) (155 mg, 0.40 mmol) and 2 drops of ethylenediamine were added to 6.0 mL of *n*-propanol/DMF (3 : 1, v/v) and mixed at room temperature. The mixed solution was heated at 100 °C for three days. After being cooled down to room temperature, red powders of racemic Ti_4L_6 cages were obtained (yield: 78% based on H_4L).

Synthesis of powder (*R*, Δ)- and (*S*, Λ)-CPM[53]

Racemic Ti_4L_6 cages (200 mg, 0.055 mmol), Mn(CH$_3$COO)$_2$·4H$_2$O (12 mg, 0.065 mmol), and (*R*)-DCH (22 μL, 0.185 mmol) were added to 6.0 mL of DMF/H$_2$O (2 : 1, v/v) and placed at room temperature (~15 °C) for 3 days. Orange crystals of (*R*, Δ)-CPM were obtained.

This compound was synthesized by substituting (*R*)-DCH with (*S*)-DCH in the above synthetic procedure for (*S*, Λ)-CPM.

Preparation of functionalized substrates

The OH-functionalized self-assembled monolayers (SAMs) on QCM working electrodes were prepared by immersing QCM substrates into 1.0 mM ethanolic solutions of 11-mercapto-1-undecanol (MUD) for 24 h and then rinsed with pure ethanol and dried under a nitrogen flux for the next preparation.

The OH-terminated quartz glass substrates were washed with ethanol by sonication in sequence. Then the substrates were cleaned with deionized water and then immersed into 0.20 M NaOH/H$_2$O$_2$ (3 : 1) solution at 80 °C for 30 min, and cleaned with deionized water and dried under a nitrogen flux for the next preparation.

Preparation of (*R*)- or (*S*)-Mn(DCH)$_3$ solution

Mn(CH$_3$COO)$_2$·4H$_2$O (36.9 mg, 0.20 mmol) and (*R*)- or (*S*)-DCH (71.3 μL, 0.60 mmol) were added to 1.0 L ethanol, and then the mixed solution was ultrasonicated for 15 minutes for further use.

In situ LPE lbl growth of (*R*, Δ)- and (*S*, Λ)-CPM films

The samples used in the present work were grown using the liquid-phase epitaxy (LPE) autoarm immersion layer-by-layer method and were fabricated using the following diluted ethanolic solutions: (*R*)- or (*S*)-Mn(DCH)$_3$ (0.20 mM) and racemic Ti_4L_6 cages (0.10 mM). The immersion times were 15 min for the (*R*)- or (*S*)-Mn(DCH)$_3$ solution and 20 min for the racemic Ti_4L_6 cage solution. Each step was washed with pure ethanol to remove residual reactants. The above details were for one growth cycle of the process. A total of 20, 30 and 40 growth cycles were used for (*R*, Δ)- and (*S*, Λ)-CPM films grown on quartz glasses in this work.

QCM adsorption of (*R*, Δ)- and (*S*, Λ)-CPM films

A commercial QCM 200 with a flow module for measurements in the gas phase was used to monitor the mass uptake and adsorption rate of the present (*R*, Δ)- and (*S*, Λ)-CPM films. CPM films were prepared on MUD SAM functionalized QCM working electrodes. The QCM can be used in gas-phase environments for monitoring the resonance frequency changes on the electrode. A decrease of the resonance frequency is ascribed to the increase of the mass on the QCM sensor according to eqn (2),

$$\Delta f_n = -nC\Delta M_f \quad (2)$$

where f_n is the resonance frequency, M_f is the mass of the crystal, and C is the mass sensitivity constant.

Author contributions

Z.-G. G. and J. Z. designed research; H. C. performed research; H. C. and Z.-G. G. analyzed data; and H. C., Z.-G. G. and J. Z. wrote the paper.

Conflicts of interest

There are no conflicts to declare.

Acknowledgements

This work was supported by the National Natural Science Foundation of China (21872148, 21935010 and 21601189) and the Youth Innovation Promotion Association of Chinese Academy of Sciences (2018339).

Notes and references

1 C.-Y. Sun, C. Qin, C.-G. Wang, Z.-M. Su, S. Wang, X.-L. Wang, G.-S. Yang, K.-Z. Shao, Y.-Q. Lan and E.-B. Wang, *Adv. Mater.*, 2011, **23**, 5629–5632.
2 T. Chen, S.-Y. Li, D. Wang and L.-J. Wan, *Sci. Adv.*, 2017, **3**, 1701208–1701215.
3 L.-J. Chen, H.-B. Yang and M. Shionoya, *Chem. Soc. Rev.*, 2017, **46**, 2555–2576.
4 M. H. Liu, L. Zhang and T. Wang, *Chem. Rev.*, 2015, **115**, 7304–7397.
5 N. S. Bobbitt, M. L. Mendonca, A. J. Howarth, T. Islamoglu, J. T. Hupp, O. K. Farha and R. Q. Snurr, *Chem. Soc. Rev.*, 2017, **46**, 3357–3385.
6 X. Zhao, Y. X. Wang, D.-S. Li, X. H. Bu and P. Y. Feng, *Adv. Mater.*, 2018, **30**, 1705189–1705222.
7 W. L. Shang, X. F. Zhu, T. L. Liang, C. Du, L. Y. Hu, T. S. Li and M. H. Liu, *Angew. Chem., Int. Ed.*, 2020, **59**, 12811–12816.
8 Z. B. Bao, G. G. Chang, H. B. Xing, R. Krishna, Q. L. Ren and B. L. Chen, *Energy Environ. Sci.*, 2016, **9**, 3612–3641.
9 K. S. Jeong, Y. B. Go, S. M. Shin, S. J. Lee, J. Kim, O. M. Yaghi and N. Jeong, *Chem. Sci.*, 2011, **2**, 877–882.
10 M. C. di Gregorio, L. J. W. Shimon, V. Brumfeld, L. Houben, M. Lahav and M. E. van der Boom, *Nat. Commun.*, 2020, **11**, 380–388.
11 X. Han, J. Zhang, J. J. Huang, X. W. Wu, D. Q. Yuan, Y. Liu and Y. Cui, *Nat. Commun.*, 2018, **9**, 1294–1303.
12 H. L. Qian, C. X. Yang and X. P. Yan, *Nat. Commun.*, 2016, **7**, 12104–12110.
13 L. K. Wang, J. J. Zhou, Y. B. Lan, S. Y. Ding, W. Yu and W. Wang, *Angew. Chem., Int. Ed.*, 2019, **58**, 9443–9447.
14 D. Luo, X. P. Zhou and D. Li, *Angew. Chem., Int. Ed.*, 2015, **54**, 6190–6195.
15 Y. W. Li, Q. F. Li, X. R. Miao, C. Y. Qin, D. Chu and L. P. Cao, *Angew. Chem., Int. Ed.*, 2021, **60**, 6744–6751.
16 J. Tian, H. Wang, D.-W. Zhang, Y. Liu and Z.-T. Li, *Natl. Sci. Rev.*, 2017, **4**, 426–436.
17 Y. H. Lu, H. C. Zhang, J. Y. Chan, R. W. Qu, H. J. Zhu, M. Forsyth, E. M. Marijanovic, C. M. Doherty, P. J. Marriott, M. M. B. Holl and H. T. Wang, *Angew. Chem., Int. Ed.*, 2019, **131**, 2–10.
18 Z.-G. Gu, C. H. Zhan, J. Zhang and X. H. Bu, *Chem. Soc. Rev.*, 2016, **45**, 3122–3144.
19 J. S. Zhao, H. W. Li, Y. Z. Han, R. Li, X. S. Ding, X. Feng and B. Wang, *J. Mater. Chem. A*, 2015, **3**, 12145–12148.
20 G. Li, W. B. Yu, J. Ni, T. F. Liu, Y. Liu, E. H. Sheng and Y. Cui, *Angew. Chem., Int. Ed.*, 2008, **120**, 1265–1269.
21 J. Q. Dong, C. X. Tan, K. Zhang, Y. Liu, P. J. Low, J. W. Jiang and Y. Cui, *J. Am. Chem. Soc.*, 2017, **139**, 1554–1564.
22 G. Li, W. B. Yu and Y. Cui, *J. Am. Chem. Soc.*, 2008, **130**, 4582–4583.
23 Y.-P. He, L.-B. Yuan, G. H. Chen, Q. P. Lin, F. Wang, L. Zhang and J. Zhang, *J. Am. Chem. Soc.*, 2017, **139**, 16845–16851.
24 J. Zhang, X. Han, X. W. Wu, Y. Liu and Y. Cui, *J. Am. Chem. Soc.*, 2017, **139**, 8277–8285.
25 X. Z. Li, J. G. Wu, C. He, Q. T. Meng and C. Y. Duan, *Small*, 2019, **15**, 1804770–1804795.
26 T. L. Li, T. Li, M. Linseis, F. S. Wang, R. F. Winter and R. R. Schmidt, *ACS Catal.*, 2020, **15**, 11406–11416.
27 D.-J. Li, Z.-G. Gu and J. Zhang, *Chem. Sci.*, 2020, **11**, 1935–1942.
28 J. L. Han, D. Yang, X. Jin, Y. Q. Jiang, M. H. Liu and P. F. Duan, *Angew. Chem., Int. Ed.*, 2019, **58**, 7013–7019.
29 C. Zhang, Z.-P. Yan, X.-Y. Dong, Z. Han, S. Li, T. Fu, Y.-Y. Zhu, Y.-X. Zheng, Y.-Y. Niu and S.-Q. Zang, *Adv. Mater.*, 2020, **32**, 2002914–2002925.
30 M. Ashford, *Drug Delivery Transl. Res.*, 2020, **10**, 1888–1894.
31 R. S. Li, P. F. Gao, H. Z. Zhang, L. L. Zheng, C. M. Li, J. Wang, Y. F. Li, F. Liu, N. Li and C. Z. Huang, *Chem. Sci.*, 2017, **8**, 6829–6835.
32 H. Xu, J. Gao and D. L. Jiang, *Nat. Chem.*, 2015, **7**, 905–912.
33 B. Yang, X.-D. Zhang, J. Li, J. Tian, Y.-P. Wu, F.-X. Yu, R. Wang, H. Wang, D.-W. Zhang, Y. Liu, L. Zhou and Z.-T. Li, *CCS Chem.*, 2019, **1**, 156–165.
34 R. J. Dong, Y. F. Zhou, X. H. Huang, X. Y. Zhu, Y. F. Lu and J. Shen, *Adv. Mater.*, 2015, **27**, 498–526.
35 B. Liu, O. Shekhah, H. K. Arslan, J. Liu, C. Wöll and R. A. Fischer, *Angew. Chem., Int. Ed.*, 2012, **51**, 807–810.
36 L. Heinke and C. Wöll, *Adv. Mater.*, 2019, **31**, 1806324–1806335.
37 Q.-P. Zhang, Z. Wang, Z.-W. Zhang, T.-L. Zhai, J.-J. Chen, H. Ma, B. Tan and C. Zhang, *Angew. Chem., Int. Ed.*, 2021, **60**, 1–6.
38 R. Kaminker, X. de Hatten, M. Lahav, F. Lupo, A. Gulino, G. Evmenenko, P. Dutta, C. Browne, J. R. Nitschke and M. E. van der Boom, *J. Am. Chem. Soc.*, 2013, **135**, 17052–17059.
39 Z.-G. Gu, W.-Q. Fu, M. Liu and J. Zhang, *Chem. Commun.*, 2017, **53**, 1470–1473.
40 S. Okur, P. Qin, A. Chandresh, C. Li, Z. J. Zhang, U. Lemmer and L. Heinke, *Angew. Chem., Int. Ed.*, 2021, **60**, 3566–3571.
41 X. K. Pei, H.-B. Burgi, E. A. Kapustin, Y. Z. Liu and O. M. Yaghi, *J. Am. Chem. Soc.*, 2019, **141**, 18862–18869.
42 C. Li and L. Heinke, *Symmetry*, 2020, **12**, 686.

43 H. H. Huo, B. j. Gorsline and G. C. Fu, *Science*, 2020, **367**, 559–564.
44 B. Bhaskararao and R. B. Sunoj, *ACS Catal.*, 2017, **7**, 6675–6685.
45 X. P. Feng, B. Shen, B. Sun, J. Kim, X. Liu and M. Lee, *Angew. Chem., Int. Ed.*, 2020, **59**, 11355–11359.
46 X. Z. Kou, Q. H. Shao, C. H. Ye, G. Q. Yang and W. B. Zhang, *J. Am. Chem. Soc.*, 2018, **140**, 7587–7597.
47 K. Wu, K. Li, Y.-J. Hou, M. Pan, L.-Y. Zhang, L. Chen and C.-Y. Su, *Nat. Commun.*, 2016, **7**, 10487.
48 F. J. Rizzuto and J. R. Nitschke, *Nat. Chem.*, 2017, **9**, 903–908.
49 L. Shao, B. Hua, X. Q. Hu, D. Stalla, S. P. Kelley and J. L. Atwood, *J. Am. Chem. Soc.*, 2020, **142**, 7270–7275.
50 J. Fu, B. Zheng, H. Z. Zhang, Y. X. Zhao, D. Zhang, W. Y. Zhang, X.-J. Yang and B. Wu, *Chem. Commun.*, 2020, **56**, 2475–2478.
51 B. Y. Li, B. Zheng, W. Y. Zhang, D. Zhang, X.-J. Yang and B. Wu, *J. Am. Chem. Soc.*, 2020, **142**, 6304–6311.
52 Y. Y. Zhou, H. F. Li, T. Y. Zhu, T. Gao and P. F. Yan, *J. Am. Chem. Soc.*, 2019, **141**, 19634–19643.
53 Y.-P. He, L.-B. Yuan, J.-S. Song, G.-H. Chen, Q. P. Lin, C. Li, L. Zhang and J. Zhang, *Chem. Mater.*, 2018, **30**, 7769–7775.
54 O. Shekhah, H. Wang, S. Kowarik, F. Schreiber, M. Paulus, M. Tolan, C. Sternemann, F. Evers, D. Zacher, R. A. Fischer and C. Wöll, *J. Am. Chem. Soc.*, 2007, **129**, 15118–15119.
55 Z.-G. Gu and J. Zhang, *Coord. Chem. Rev.*, 2019, **378**, 513–532.
56 Z.-G. Gu, A. Pfriem, S. Hamsch, H. Breitwieser, J. Wohlgemuth, L. Heinke, H. Gliemann and C. Wöll, *Microporous Mesoporous Mater.*, 2015, **211**, 82–87.
57 B. Ishimoto, K. Tonam and S. Ikawa, *Spectrochim. Acta, Part A*, 1999, **55**, 2321–2327.
58 Q. Sun, M. Liu, K. Y. Li, Y. Han, Y. Zuo, F. F. Chai, C. S. Song, G. L. Zhang and X. W. Guo, *Inorg. Chem. Front.*, 2017, **4**, 144–153.